Journal of
Ceramic Science
and Technology

J. Ceram. Sci. Tech., 07 [02] 173-182 (2016)
DOI: 10.4416/JCST2016-00010
available online at: http://www.ceramic-science.com

Thermal Shock Performance of Refractories for Application in Steel Ingot Casting

J. Fruhstorfer*[1], S. Schafföner[1], J. Werner[1], T. Wetzig[1], L. Schöttler[2], C.G. Aneziris[1]

[1]Institute of Ceramic, Glass and Construction Materials, TU Bergakademie Freiberg, Agricolastraße 17, 09599 Freiberg, Germans
[2]Deutsche Edelstahlwerke GmbH, Obere Kaiserstraße, 57078 Siegen, Germany
received January 25, 2016; received in revised form March 19, 2016; accepted April 6, 2016

Abstract

This study investigates the thermal shock performance of carbon-free and low-carbon-containing refractories, with and without nanoscale additives, based on alumina, mullite, and alumina doped with zirconia and titania (AZT). For this purpose, the porosity and cold modulus of rupture of the refractories before and after a single thermal shock by compressed air were determined. The mullite-matrix materials exhibited the highest porosities owing to restrained densification during sintering, but exhibited the lowest strength losses of the carbon-free materials. In general, the carbon-containing materials had very low strengths because the carbon content was only 4 wt%. The matrix strength was therefore quite low. However, the additions of nanoadditives increased the strength of the carbon-containing alumina. Meanwhile, in the carbon-containing mullite, the nanoadditives caused an enhanced reaction of the used mullite raw material, while in the carbon-containing AZT, the nanoadditives resulted in enhanced decomposition of the aluminum titanate phase — leading to reduced strengths after thermal shock. Nevertheless, all alumina-based compositions as well as the carbon-free mullite-matrix materials seem very promising for application in steel ingot casting.

Keywords: Thermal shock resistance, nanoadditives, mullite, alumina-titania-zirconia, fused raw material

I. Introduction

Non-metallic inclusions act as stress raisers and significantly impair the mechanical properties of ingot-cast steels. These inclusions often arise from chemical and mechanical interaction of the steel with refractories. Thus, to reduce non-metallic inclusions and to meet the steel quality requirements, high-alumina, mullite and zirconia [1–3] as well as carbon-bonded refractories [4] have been recently developed as alternatives to traditional fireclay refractories for steel ingot casting applications [1,5].

Steels for special applications and steel grades that are sensitive to the severe bending stresses occurring at high temperatures during continuous casting are ingot-cast discontinuously. In a previous study [6], the corrosion of alumina refractories was investigated as a function of the ingot-casting steel composition and its casting temperature. The tested steels were 100CrMn6 with high Si and C contents, X10MnCrN1818 with high Mn and Cr contents, X5CrNiCuNb174 with a high Cr content as well as 18CrNiMo7–6 with a high casting temperature of 1580 °C. The corrosion increased as a function of the aluminum content of the steels and of the casting temperature. Since the most severe attack was caused by the steel 18CrNiMo7–6, it was chosen for further corrosion experiments.

Ingot casting is usually performed in a bottom teeming process by pouring the steel through refractory pipes (hollowware) into the ingot mold. The whole refractory system is not preheated. The disposable hollowware, such as runner and spider bricks, is thus exposed to a single thermal shock as well as to hot erosion and corrosion owing to the steel flow. The exposure time is about 15–45 minutes until the steel solidifies [1,4].

The refractory hollowware, such as runner bricks, is produced by means of extrusion or increasingly also by upright die pressing [2–4]. More complex shapes such as spider bricks are manufactured by means of extrusion with post-processing or by casting processes.

During extrusion and upright die pressing, high friction occurs between the tool walls and the refractory mass as well as in the mass itself. To reduce the friction, considerable amounts of plasticizing clay with high contents of SiO_2 are used [3,4]. The SiO_2, however, later reacts with alloy elements of the steel such as manganese, chromium or aluminum [1–5,7]. Upright die pressing of runner bricks with a reduced clay content was consequently proposed in a previous study [8]. The upright die pressing was successful owing to increased lubrication with the application of an additive mix of a polysaccharide binder, a high-viscous cellulose derivative plasticizer, a fatty acid lubricant and a

* Corresponding author: jens.fruhstorfer@ikgb.tu-freiberg.de

wax dispersion pressing aid together with water as the dispersing medium.

Moreover, particle size distributions of alumina castables for the later manufacturing of spider bricks were investigated by modifying the Andreasen particle size distribution model [9], which is usually used to optimize refractory castable batches. The novel approach introduced by Fruhstorfer and Aneziris [10] allowed separate adjustment of the amount of fine and coarse particle fractions by adjusting the values of the minimum and maximum distribution modulus n_{min} and n_{max}, respectively. A particle size design independent of the refractory raw material was found which simultaneously optimizes flowability, stability, density and pore sizes. In a following study [6], refined input parameters ($n_{min} = 0.27$, $n_{max} = 0.8$) of the new model were used, which further improved flowability and minimized maximum pore sizes.

Pure alumina has unsatisfactory thermal shock resistance for application in steel ingot casting. Thus, fine-grained alumina doped with 2.5 wt% zirconia and 2.5 wt% titania (AZT) was investigated because AZT has high potential to resist thermal shock due to complex microcrack networks [11,12]. However, in a previous study [13], it was found that AZT may reach its full potential to resist thermal shock only for particle sizes below 63 μm and an open porosity below 20 %. Furthermore, sintering temperatures above 1300 °C were beneficial if the raw material contained unconverted reactants of the aluminum titanate formation.

Additionally, mullite and zirconia as well as carbon-bonded refractories have also been recently investigated besides alumina materials for application in steel ingot casting [1,4]. Carbon-containing refractories are highly resistant to thermal shock [14] and corrosion caused by steel and slag melts [15]. Nevertheless, owing to a concern of carbon contamination of the steel melt and ecological concerns, a reduction of the carbon content is of great interest [16,17]. Roungos *et al.* [17,18] reported that the thermomechanical properties can be kept on a high level or can even be improved for a reduced carbon content if the carbon matrix is reinforced with carbon nanotubes and alumina nanosheets.

The presented literature survey points out that there is a wide range of applied and tested materials. For that reason, the latest previous study [19] compared comprehensively the corrosion of refractories for application in steel ingot casting by an aggressive steel (1.6587, 18CrNiMo7–6) [6] in order to evaluate the best material in respect of corrosion resistance. The tested refractories were based on carbon-free or low-carbon-containing alumina, mullite and zirconia- and titania-doped alumina (AZT) with and without nanoscale additives. The most promising materials for application in steel ingot casting were the carbon-containing refractories and the mullite-matrix materials. The carbon-containing refractories were only negligibly corroded and the carbon-free mullite-matrix materials showed only very low corrosion due to the formation of a high-viscous melt at the steel-refractory-interface.

In this previous study, a comprehensive comparison of potential refractory materials regarding the corrosion requirement was conducted. Nevertheless, besides corrosion resistance, the refractories also need excellent erosion and thermal shock resistance. However, to the best of the authors' knowledge a comparison of these materials regarding their resistance to a single thermal shock has not yet been conducted.

Thus, the purpose of this study is to compare the thermal shock resistance of carbon-free and low-carbon-containing refractories with and without nanoscale additives based on alumina, mullite, and AZT materials.

II. Experimental

To investigate the thermal shock resistance of refractories for application in steel ingot casting, standard refractory bars were die-pressed and their strengths measured before and after a single thermal shock.

(1) Materials and compositions

The investigated refractories were based on the oxidic-matrix materials alumina, fused mullite and fused alumina doped with 2.5 wt% zirconia and 2.5 wt% titania (AZT). The AZT had been previously treated for 12 h at 700 °C to burn out the residual carbon from the fusion process and was only used in the finest fraction according to Fruhstorfer *et al.* [13]. The nanoscale additives were characterized in a preceding study by Roungos *et al.* [18]. Relevant details of the raw materials are listed in Table 1.

For the following calculation of the batch distributions, the particle size distributions and true densities of the separate grain fractions were determined according to the standards DIN EN 725–5, DIN 66165–2 and DIN 66137–2.

The compositions of the pressing masses were designed in line with the modified Andreasen model introduced by Fruhstorfer and Aneziris [10] for a minimum distribution modulus of 0.2 and a maximum one of 0.8 to increase the sintering mismatch of fine and coarse fractions, which generally improves thermal shock resistance [20]. The particle size distributions were designed primarily to have similar volume distributions and only secondarily to follow the mathematically described curve to improve the later comparison of the properties. In the finest fractions below ≈ 5 μm, therefore, the actually attained and theoretical particle size distributions differ to some extent. Table 1 lists the final compositions of the carbon-free and -containing masses with and without nanoscale additives.

The true densities of the complete batches in fired state as listed in Table 1 were calculated from the true densities of the raw materials. Besides the measured true densities of the grain fractions, densities of 1.3 gcm^{-3} and 0.85 gcm^{-3}, respectively, were considered for the components of the resin (solid bakelite and an organic solvent) [21].

Carbon-bonded refractories are generally not wetted by molten steel and slags and thus their corrosion is inhibited. In this study the carbon contents were reduced to the lowest level, which allows the formation of a continuous carbon-bonded matrix which covers the oxidic grains like a closed-cell foam. According

to Gibson [22], closed-cell foams can be manufactured with as low as 9 vol% relative density. An addition of about 4 wt% carbon-containing raw materials can result in up to 10 vol% residual carbon after coking according to Fruhstorfer *et al.* [19]. In this previous study, a modified coal tar pitch was used which has a minimum coking value of 80 %. In the present study, a resin with a slightly lower coking value was used. The amounts in the different batches were adjusted to attain similar volume fractions of the resin after coking. However, a pure carbon bond cannot be guaranteed and thus the possibility of connected oxidic grains that sinter during thermal treatment cannot be excluded. The corresponding samples are therefore indicated as carbon-containing and not as carbon-bonded materials.

Table 1: Compositions in wt% of the pressed bars (A – Alumina, M – Mullite, AZT – 2.5 wt% zirconia- and 2.5 wt% titania-doped alumina, C – Carbon, n – Nanoadditives).

Function	Raw material	Fraction in mm	Pressing mass types										
			A	A-C	A-C-n	A-M	M	M-C	M-C-n	M-A	AZT-A	AZT-A-C	AZT-A-C-n
Graining	Tabular alumina T 60/64[a]	1—3	35	35	35	20				40	35	35	35
		0.5—1	5	5	5					5	5	5	5
		0–0.5	5	5	5	10					5	5	5
		0–0.2	15	15	15	10							
		0–0.045	30	30	30	35							
		0–0.02	10	10	10	10	10	10	10	10	10	10	10
	Sinter mullite Symulox M72[b]	1.5—3				15	35	35	35				
		0.5—1.5					5	5	5				
	Fused mullite Alodur WFM[c]	0–0.5					5	5	5	5			
		0–0.15					45	45	45	40			
	Slowly cooled fused AZT	0–0.045									45	45	45
Binder	Zusoplast WE 52[e]		2.5			2.58	3.04			2.77	2.45		
Resin	Bakelite PF 0235 DP[f]			1	1			1.21	1.21			0.98	0.98
	Bakelite PF 6662 FL 01[f,*]			3	3			3.65	3.65			2.95	2.95
Hardener	Hexamethylenetetramine[f]			0.4	0.4			0.49	0.49			0.39	0.39
Nano-additive	Multi-walled carbon nanotubes[g]				0.1				0.1				0.1
	Alumina nanosheets[h]				0.3				0.3				0.3
Calculations	True densities (fired) in gcm^{-3}		3.794	3.477	3.476	3.665	3.121	2.879	2.881	3.423	3.866	3.540	3.539
	Nanoadditives in vol%				0.4106				0.3380				0.4184

Suppliers: [a]Almatis, [b]Nabaltec, [c]Imerys Fused Minerals, [d]C.A.R.R.D., [e]Zschimmer & Schwarz, [f] Momentive Specialty Chemicals, [g]Timesnano, [h]Sawyer

* nonvolatile content of Bakelite PF 6662 FL 01 typically 77% according to manufacturer

(2) Sample preparation and testing

The batches were prepared by means of ordered mixing [23] using a conventional mortar mixer (ToniMIX, Toni Baustoffprüfsysteme GmbH, Germany). Firstly, the coarse grains larger than 0.5 mm were dry-mixed for 1 min. Then the pressing aid for carbon-free and the resin for the carbon-containing batches was added and mixed for 5 min. Then the finer grain fractions and remaining additives were added. The batch was then mixed again for 3 min before the walls of the mixing container were scraped and the mix was further stirred a last time for 7 min.

Six bars (150 x 25 x 25 mm^3) of each composition were pressed on a uniaxial press (ES 270, RUCKS Maschinenbau GmbH, Germany) at 80 MPa. To avoid cracks caused by entrapped air, the pressure was released at one third and two thirds of the maximum pressure.

The carbon-free samples were sintered with a heating rate of 1 K/min to 600 °C and with 2 K/min to the sintering temperature, which was held 1.5 h before the samples were cooled with 2 K/min to 800 °C. The sintering temperature of the alumina- and mullite-matrix samples was 1600 °C. For the AZT-containing masses, two sintering temperatures were used. Six samples were sintered at 980 °C because preliminary experiments had determined that the maximum of the refractoriness under load (standard DIN EN 993 – 8) curve of samples containing 25 wt% AZT was only 1090.2 °C. These experiments resembled the behavior of large samples during sintering. However, in a previous study [13] the best thermomechanical properties of fine-grained AZT were obtained after sintering at 1650 °C, which was therefore used as the second sintering temperature and for comparison.

The carbon-containing samples were cured before coking by gradually increasing the temperature to 180 °C with a following dwell time of 90 min similar to the curing conditions described by Mertke and Aneziris [24]. Later on, the cured samples were fired in retorts filled with coke to ensure a reducing atmosphere. The samples were heated with 3 K/min to 1000 °C followed by a dwell time of 5 h as previously reported [18].

After firing, the bulk density of all specimens was determined on six bars from the samples' dimensions and mass. Furthermore, the cold moduli of rupture (CMOR) were measured on three samples according to the standard DIN EN 993 – 6 in a 3-point bending test (TIRAtest 2420, TIRA GmbH, Germany). Then, the remaining three samples were quenched for a single time from 950 °C according to the standard DIN EN 993 – 11 using compressed air. Afterwards, their retained CMOR was measured and compared to the one of the non-quenched samples. For exemplary microstructure analysis, samples were prepared for scanning electron microscopy (SEM) (ESEM XL30FEG, FEI company, Netherlands) combined with energy-dispersive X-ray spectrometry (EDX) (EDAX, Ametek GmbH, Germany).

III. Results and Discussion

To compare the suitability of different refractory materials for application in steel ingot casting, their resistance to a single thermal shock was compared. For this purpose, carbon-free and carbon-containing refractories with and without nanoscale additives based on alumina, mullite, and alumina doped with zirconia and titania (AZT) were prepared.

Table 2 shows the means and standard deviations of the determined bulk densities, porosities, cold moduli of rupture before ($CMOR_{0TS}$) and after ($CMOR_{1TS}$) thermal shock (TS) as well as the strength losses with TS. The porosities were determined from the measured bulk densities and the calculated true densities stated in Table 1. The mean percental strength losses with TS were calculated as $100\,\% \cdot (CMOR_{0TS} - CMOR_{1TS})/CMOR_{0TS}$.

To analyze the results of the experimental design, the discussion was split into three parts: Firstly, the carbon-free materials were compared. Then the comparison of the carbon-free with the carbon-containing alumina, mullite, and AZT materials followed and then the effect of the nanoscale additives in carbon-containing alumina, mullite, and AZT materials was evaluated.

(1) Carbon-free materials

The average porosities of the ceramic-bonded materials are presented in Fig. 1(a). The porosity of the AZT-matrix material decreased strongly with increasing sintering temperature. In comparison to the alumina-matrix materials (≈ 23 % porosity), the porosity of the AZT sintered at 1650 °C (≈ 20 %) was comparatively low. The titania component presumably affected densification and grain growth as a result by grain boundary action, as concluded by McKee and Aleshin [25]. The mullite-matrix materials had the highest porosities of about 28 to 29 %. Mullite-matrix materials have to be fired at temperatures ≥ 1650 °C during pressureless sintering to achieve densification [26] because the sintering of mullite has a high activation energy of about 700 kJ/mol [27]. For comparison, the sintering activation energy of other oxide ceramics is commonly around 500 kJ/mol [28]. The mullite densification was thus probably restrained in comparison to the alumina- and AZT-matrix materials.

Fig. 1(b) presents the CMOR of the thermal-shocked carbon-free specimen. The initial strengths behaved conversely to the porosities, similar to that reported by Coble and Kingery [29]. Only the AZT-matrix material sintered at lower temperature (AZT-A-980) had comparatively low strengths due to its insufficient densification and bonding between the coarser alumina particles. The loss in strength of 45 to 60 % was highest for the pure alumina and the AZT-matrix materials sintered at lower temperature (AZT-A-980), respectively. The AZT-matrix material sintered at higher temperature (AZT-A-1650) had a lower strength loss than the pure alumina. Furthermore, this obtained strength loss (≈ 46 %) was lower than the one reported in a previous study [13] of 62 %. In the present study the porosity was lower with about 20 % than in the preceding contribution (22 %). Thus, a further reduction of the porosity may lead to a further improvement in thermal shock performance. However, it should be mentioned again that due to the less than perfect refractoriness under load behavior only samples of limited dimensions can be sintered at this high temperature.

Table 2: Properties of the regarded materials (A – Alumina, M – Mullite, AZT – 2.5 wt% zirconia- and 2.5 wt% titania-doped alumina)

Batch	Factors of exp. design			Measurements				
	Material basis	Carbon content	Nano-add.	Bulk density in gcm^{-3}	Porosity in vol%	$CMOR_{0TS}$ in MPa	$CMOR_{1TS}$ in MPa	Strength loss in %
A	A	free	no	2.91 ± 0.01	23.25 ± 0.37	10.01 ± 1.41	4.82 ± 0.44	51.8
A-C		containing	no	2.88 ± 0.02	17.14 ± 0.55	2.38 ± 0.57	2.32 ± 0.09	2.5
A-C-n			yes	2.88 ± 0.02	17.07 ± 0.56	3.81 ± 1.29	3.06 ± 0.93	19.7
A-M	A-M	free	no	2.83 ± 0.03	22.69 ± 0.73	8.35 ± 1.75	7.63 ± 1.00	8.6
M	M	free	no	2.23 ± 0.01	28.65 ± 0.37	4.49 ± 0.55	2.77 ± 0.26	38.3
M-C		containing	no	2.28 ± 0.01	20.66 ± 0.27	2.18 ± 0.21	1.88 ± 0.19	13.8
M-C-n			yes	2.28 ± 0.01	20.88 ± 0.45	1.46 ± 0.58	0.86 ± 0.30	41.1
M-A	M-A	free	no	2.46 ± 0.01	27.99 ± 0.41	4.01 ± 0.19	3.28 ± 0.50	18.2
AZT-A-980[a]	AZT-A	free	no	2.90 ± 0.02	25.09 ± 0.50	0.54 ± 0.03	0.22 ± 0.04	59.3
AZT-A-1650[b]				3.09 ± 0.02	19.87 ± 0.48	11.15 ± 1.35	6.05 ± 0.76	45.7
AZT-A-C		containing	no	2.90 ± 0.02	18.01 ± 0.58	2.06 ± 0.45	1.43 ± 0.45	30.6
AZT-A-C-n			yes	2.88 ± 0.03	18.52 ± 0.80	2.26 ± 0.40	0.93 ± 0.38	58.8

[a] Sintering temperature 980 ° C

[b] Sintering temperature 1650 °C

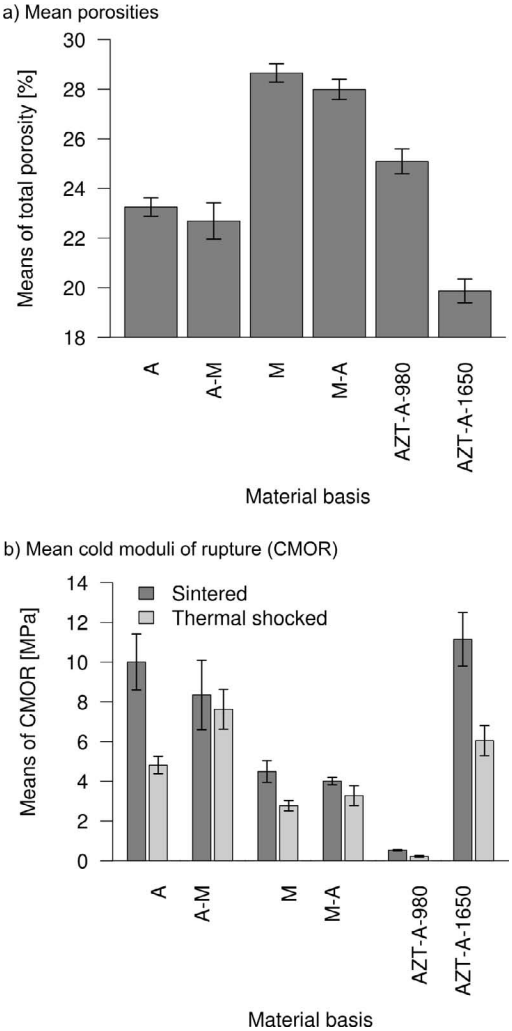

Fig. 1: Properties of the carbon-free materials (labels according to batch names in Table 2).

The carbon-free mullite-containing samples had the lowest strength losses with values below 40 %. The material with the highest residual strength after thermal shock of ≈ 8 MPa and the lowest strength loss of ≈ 9 % were the alumina-mullite specimen with alumina matrix. These superior properties of alumina-mullite and mullite-alumina materials can be most probably attributed to a microcrack network, which results from the thermal expansion mismatch of these two phases during sintering [30]. Thus, they had lower initial strengths than the corresponding pure materials, but higher retained strengths after thermal shock. Furthermore, the development of the microcrack network was enhanced by the applied particle size distribution of the raw materials as described in the Experimental section.

(2) Carbon-free and carbon-containing alumina, mullite, and AZT materials

The porosities are shown in Fig. 2(a). It can be seen that, generally, the carbon-containing materials had a lower porosity than the carbon-free materials. A possible reason could be that during coking fewer components burn out than during sintering. A further reason might be that the lubrication during compaction was improved for the carbon-containing samples due to the higher amount of resin in the carbon-containing samples compared to the pressing aid content in the carbon-free samples. An improved lubrication leads to an increased densification [8].

Nevertheless, the AZT-A-C specimen had higher porosities than the A-C specimen. The aluminum titanate presumably decomposed under reducing conditions [31],

which leads to an increasing porosity [13]. The comparatively high porosity of the carbon-containing mullite could either be explained by a restrained densification (see prior subsection) if it is assumed that the carbon content was so low that still partial sintering occurred. On the other hand, in the particle fractions with sizes below 0.5 mm only fused mullite was used, cf. Table 1, but it was found by EDX analysis that the fused 2:1 mullite partially transformed into 3:2 mullite as will be shown in detail in the following subsection. The reaction of 2:1 to 3:2 mullite is accompanied by an increase in density from about 3.14 gcm^{-3} to 3.19 gcm^{-3} [28], leading to shrinkage of the mullite grains and thus to an increased porosity of the complete refractory sample.

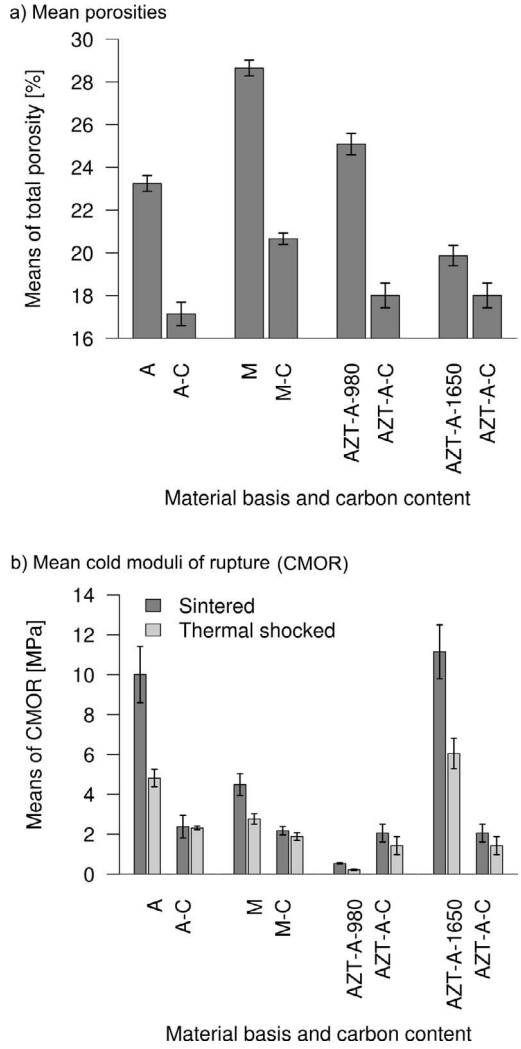

Fig. 2: Properties of the carbon-free and carbon-containing alumina, mullite, and AZT materials (labels according to batch names in Table 2)

Fig. 2(b) presents the CMOR before and after thermal shock depending on the raw material and the carbon content. Generally, the carbon-containing samples had lower strengths than their ceramic-bonded equivalents. The carbon-free samples densified by sintering whereas the carbon in the carbon-containing ones polymerized and formed an at least partial carbon matrix. The carbon matrix separates the oxidic grains from each other and, thus, no sintering occurs between the oxidic grains. The carbon matrix also shrinks less during thermal treatment and, therefore, more grains displace [32] than in ceramic-bonded systems where in the matrix the fine particles sinter. Therefore, the strengths of the carbon-containing specimen were lower than the ones of their carbon-free equivalents.

Furthermore, since the carbon addition was very low, the ligament widths of the closed-cell foam-like matrix structure were probably very thin and weak, which causes a low strength. The low carbon content together with the low strength of the carbon matrix might also explain the very low scattering of the means of CMOR of the carbon-containing samples (2.06 to 2.32 MPa) before thermal shock. In contrast, the strengths of the ceramic-bonded materials depended strongly on the material type owing to different porosity levels and sintering densifications. Thus, it can be concluded that the carbon matrix in the carbon-containing batches dominated a possibly partial carbon-free matrix insofar as the final properties are concerned.

In addition, as can be seen from Fig. 2(b), the relative loss in strength after thermal shock of the carbon-containing samples was always lower compared to the strength loss of the carbon-free materials. Carbon has a high thermal conductivity. The carbon matrix together with embedded grains forms a complex crack network. On one hand, this crack network leads to a high thermal shock resistance but on the other hand to low overall strengths. Comparing the carbon-containing samples, the A-C samples had the lowest strength loss, whereas the M-C and AZT-A-C samples had higher strength losses. As described for the analysis of the porosities, the aluminum titanate decomposition and mullite phase transformation during coking might increase the defect density to a level that could damage the microstructure, causing reduced thermal shock resistance. Furthermore, the processes respectively reactions might continue during thermal shocking.

The strengths of the carbon-free systems after thermal shock were generally higher. Nonetheless, the AZT-A samples sintered at lower temperature (AZT-A-980) had a lower strength after thermal shock due to insufficient densification. The lower strength of the carbon-containing materials after thermal shock can be also explained by their low carbon content and low strength of the carbon matrix.

(3) Carbon-containing alumina, mullite, and AZT materials with and without nanoadditives

Fig 3(a) presents the porosities of the carbon-containing materials with and without the addition of nanoadditives. It seems that the porosities of the mullite- and AZT-containing samples, in which a decomposition or phase transformation presumably occurred, were higher. However, the effect cannot be validated due to the low differences in the porosity values compared to the standard deviations, cf. Table 2.

The initial strength of the carbon-containing alumina increased with the nanoadditive addition, as also recently reported [18]. However, adding the nanoadditives to the AZT material had nearly no effect, whereas in the mullite samples, it resulted in decreasing initial strengths. Furthermore, for all compositions the strength loss was higher with the addition of nanoadditives. In the A-C-n sample

the initial strength increased, which is commonly accompanied by a higher strength loss after thermal shock [33]. In the mullite- and AZT-containing specimen it seems that the occurring reactions were enhanced by the nanoadditives — leading to comparatively low initial strength values and high strength losses.

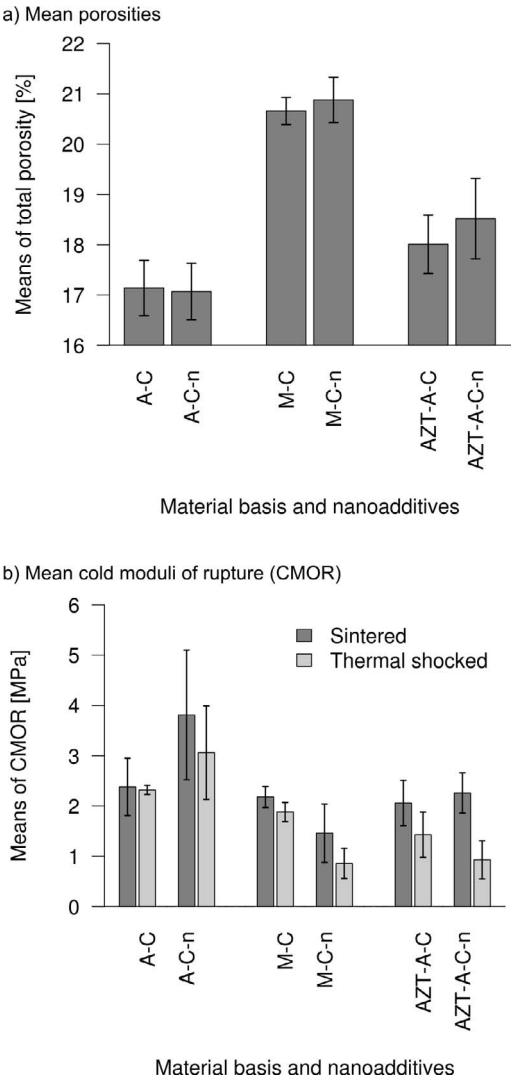

Fig. 3: Properties of the carbon-containing alumina, mullite, and AZT materials with and without nanoadditives (labels according to batch names in Table 2).

Fig. 4 shows an SEM image of an M-C-n sample after thermal shock. EDX measurements were conducted on the inside and on the surface of the two tagged grains to investigate the occurring reactions. Grain A had an inner composition of 3:2 mullite (60 mol% Al_2O_3, 39 mol% SiO_2 and 1 mol% K^2O) whereas on the surface it corresponded to 2:1 mullite (67 mol% Al_2O_3 and 33 mol% SiO_2). However, the EDX measurements on the inside and surface of grain B corresponded to an alumino-silicate (15 mol% Al_2O_3, 74 mol% SiO_2, 6 mol% Na_2O and 5 mol% K_2O). The composition of Grain B, therefore, was in line with a eutectic composition of about 12 mol% Al_2O_3 and 78 mol% SiO_2 of the metastable Al_2O_3-SiO_2 phase diagram reported by Risbud and Pask [34]. Consequently, especially the alumina nanosheets may have initiated further and enhanced reactions in the samples that contained the fused mullite raw material.

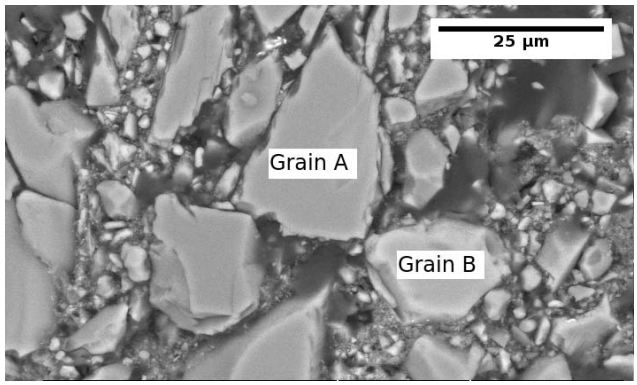

Fig. 4: SEM image of the carbon and nanoadditives containing mullite after thermal shock.

(4) Estimated requirements for application in steel ingot casting

Refractories for steel ingot casting are exposed to a severe single thermal shock which is followed by a combined attack of erosive fluid flow and physicochemical corrosion.

According to Schulle [35] the erosion resistance of refractories is sufficient for cold crushing strengths ≥ 10 MPa and open porosities below 25 %. Thus, taking a closed porosity of about 5 % into consideration, the total porosity should be below 30 %, which was the case for all regarded samples. Anyway, taking the typical relation of 5:1 of cold crushing strength to cold modulus of rupture [35] into consideration, the determined strength after thermal shock should be at least 2 MPa. However, it should be mentioned that this presumption is only a rough estimation because the ratio of the cold crushing strength to the cold modulus of rupture usually strongly depends on the microstructure.

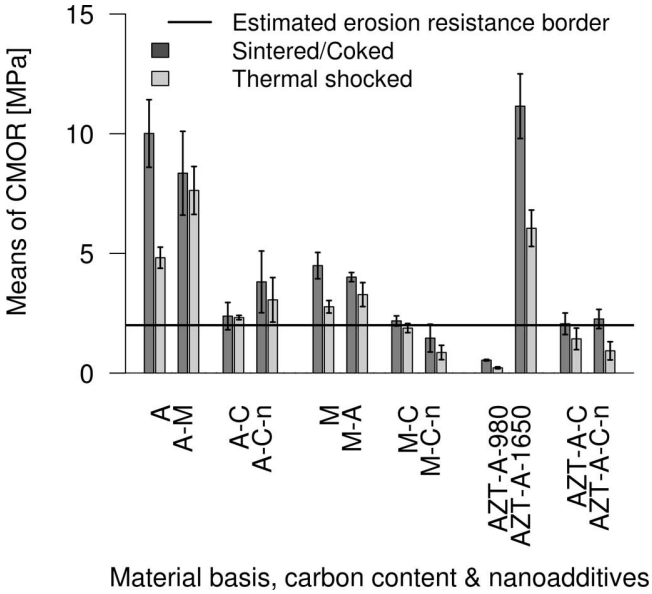

Fig. 5: Comparison of cold moduli of rupture (CMOR) before and after thermal shock for all regarded batches (labels according to batch names in Table 2).

In Fig. 5 it can be seen that the AZT- and carbon-containing mullite samples might have insufficient strengths. The AZT samples sintered at 1650 °C exhibited adequate

strength but due to a low refractoriness under load larger components cannot be produced from this material.

Regarding the corrosion, it was shown in a previous study [19] that the carbon-containing refractories and the mullite-matrix materials exhibited only slight corrosion. The most promising materials, considering both the corrosion and thermal shock resistance together, are therefore the carbon-containing alumina-based samples and the mullite-matrix materials.

IV. Conclusions

In this study the thermal shock performance of refractories for steel ingot casting was investigated. Carbon-free and low-carbon-containing refractory materials with and without nanoadditives based on alumina, mullite, and alumina doped with zirconia and titania (AZT) were considered. The following conclusions can be drawn:

- A further reduction of the porosity below 20 % might lead to a further improved thermal shock performance of AZT materials sintered at 1650 °C.
- About 4 wt% carbon addition resulted in a carbon matrix with low strength. The strength was improved to an adequate level by nanoscale additives for carbon-containing alumina.
- Fused 2:1 mullite and the aluminum titanate in the AZT material seem to decompose in reducing atmosphere. The decomposition reactions were enhanced by the nanoscale additives.
- The carbon-containing alumina-based samples and the carbon-free mullite-based samples seem promising for applications in steel ingot casting with regard to corrosion and thermal shock resistance in conjunction.

Furthermore, in addition to the corrosion behavior studied in a previous article [19], a further study will also investigate the cast steel composition and distribution of inclusions after the corrosion tests using a special Aspex-SEM. Consequently, for a final evaluation of refractories for steel ingot casting, the results from all three studies will have to be taken into consideration.

Acknowledgment

The authors thank the German Research Foundation (DFG) for supporting this collaborative study under the grant number AN 322/27 – 1. Furthermore, the authors thank Dr Schmidt for capturing the SEM images and conducting the EDX measurements.

References

[1] Zhang, L., Thomas, B.G.: State of the art in the control of inclusions during steel ingot casting, *Metall. Mater. Trans. B*, **37B**, 733 – 61, (2006).

[2] Schönwelski, W., Ruwier, K., Foellbach, S., Sperber, J.: Refractory for ingot casting of high-quality steels, in german, *stahl eisen*, **134**, [9], 58 – 62, (2014).

[3] Rettore, R.d.P., Gueguen, E., Ritter, W.: High alumina refractory material with improved thermal shock resistance and hot properties for hollowware, *The Refractories Engineer*, **November Issue,** 19 – 22, (2012).

[4] Ritter, W., Ruwier, K.G., Schönwelski, W.: Carbonaceous fireproof material for use when casting steel in a bottom casting process and formed parts produced thereof, Patent WO 2011/054872 A1, (2011).

[5] Zhang, L., Thomas, B.G.: Inclusions in continuous casting of steel, In: XXIV National Steelmaking Symposium, Morelia, Mich, Mexico, 2003.

[6] Fruhstorfer, J., Schöttler, L., Dudczig, S., Schmidt, G., Gehre, P., Aneziris, C.G.: Erosion and corrosion of alumina refractory by ingot casting steels, *J. Eur. Ceram. Soc.,* **36**, 1299 – 306, (2016).

[7] Ellingham, H.J.T.: Reducibility of oxides and sulphides in metallurgical processes, *J. Soc. Chem. Ind. (J. Chem. Technol. Biotechnol.),* **X,** 125 – 33, (1944).

[8] Fruhstorfer, J., Barlag, S., Thalheim, M., Schöttler, L., Aneziris, C.G.: Upright die pressing of refractory hollowware for steel ingot casting with reduced clay content, *Ceram. Int.,* **42**, 3219 – 28, (2016).

[9] Andreasen, A.: On the relation between grading and interstices in products of loose grains, in german, *Colloid Polym. Sci.,* **50,** 217 – 28, (1930).

[10] Fruhstorfer, J., Aneziris, C.G.: The influence of the coarse fraction on the porosity of refractory castables, *J. Ceram. Sci. Tech.,* **5**, [2], 155 – 66, (2014).

[11] Aneziris, C.G., Dudczig, S., Gerlach, N., Berek, H., Veres, D.: Thermal shock performance of fine-grained Al_2O_3 ceramics with TiO_2 and ZrO_2 additions for refractory applications, *Adv. Eng. Mater.,* **12**, [6], 478 – 85, (2010).

[12] Dudczig, S., Veres, D., Aneziris, C.G., Skiera, E., Steinbrech, R.W.: Nano- and micrometer additions of SiO_2, ZrO_2 and TiO_2 in fine-grained alumina refractory ceramics for improved thermal shock performance, *Ceram. Int.,* **38**, [3], 2011 – 9, (2012).

[13] Fruhstorfer, J., Möhmel, S., Thalheim, M., Schmidt, G., Aneziris, C.G.: Microstructure and strength of fused high alumina materials with 2.5 wt% zirconia and 2.5 wt% titania additions for refractory applications, *Ceram. Int.,* **41**, 10644 – 53, (2015).

[14] Cooper, C.F., Alexander, I.C., Hampson, C.J.: The role of graphite in the thermal shock resistance of refractories, *Br. Ceram. Trans.,* **84**, [2], 57 – 62, (1985).

[15] Lee, W.E., Zhang, S.: Melt corrosion of oxide and oxide-carbon refractories, *Int. Mater. Rev.,* **44**, [3], 77 – 104, (1999).

[16] Skiera, E., Malzbender, J., Mönch, J., Dudczig, S., Aneziris, C.G., Steinbrech, R.W.: Controlled crack propagation experiments with a novel alumina-based refractory, *Adv. Eng. Mater.,* **14**, [4], 248 – 54, (2011).

[17] Roungos, V., Aneziris, C.G., Berek, H.: Novel Al_2O_3-C refractories with less residual carbon due to nanoscaled additives for continuous steel casting applications, *Adv. Eng. Mater.,* **14**, [4], 255 – 64, (2012).

[18] Roungos, V., Aneziris, C.G.: Improved thermal shock performance of Al_2O_3-C refractories due to nanoscaled additives, *Ceram. Int.,* **38**, [2], 919 – 27, (2012).

[19] Fruhstorfer, J., Dudczig, S., Gehre, P., Schmidt, G., Brachhold, N., Schöttler, L., Aneziris, C.G.: Corrosion of carbon free and bonded refractories for application in steel ingot casting, *Steel Res. Int.*, Manuscript accepted on March 17, (2016)

[20] Lee, W.E., Zhang, S., Karakus, M.: Refractories: controlled microstructure composites for extreme environments, *J. Mater. Sci.,* **39**, 6675 – 85, (2004).

[21] Say, M.G.: 1 - Units, Mathematics and Physical Quantities. In: Laughton, M.A., Say, M.G.: Electrical Engineer's Reference Book, 14th edition. Butterworth-Heinemann, Oxford, 1985.

[22] Gibson, L.J.: Mechanical behavior of metallic foams, *Annu. Rev. Mater. Sci.,* **30**, 191 – 227, (2000).

[23] Saharan, V. A., Kukkar, V., Kataria, M., Kharb, V., Choudhury, P.K.: Ordered mixing: mechanism, process and applications in pharmaceutical formulations, *Asian J. Pharm. Sci.,* **3**, [6], 240 – 59, (2008).

[24] Mertke, A., Aneziris, C.G.: The influence of nanoparticles and functional metallic additions on the thermal shock resistance of carbon bonded alumina refractories, *Ceram. Int.,* **41,** 1541 – 52, (2015).

[25] McKee, W.D. Jr., Aleshin, E.: Aluminum oxide-titanium oxide solid solution, *J. Am. Ceram. Soc.,* **46**, [1], 54 – 8, (1963).

[26] Aksay, I.A., Dabbs, D.M., Sarikaya, M.: Mullite for structural, electronic and optical applications, *J. Am. Ceram. Soc.,* **74**, [10], 2343 – 58, (1991).

[27] Rodrigo, P.D.D., Boch, P.: High purity mullite ceramics by reaction sintering, *Int. J. High Tech. Ceram.,* **1**, 3 – 30, (1985).

[28] Salmang, H., Scholze, H.: Ceramic, in German,. 7th, completely revised and extended edition. Springer Berlin Heidelberg New York, 2007.

[29] Coble, R.L., Kingery, W.D.: Effect of porosity on physical properties of sintered alumina, *J. Am. Ceram. Soc.,* **39**, [11], 377 – 85, (1956).

[30] Ulbricht, J., Dudczig, S., Tomsu, F., Palco, S.: Technological measures to improve the thermal shock resistance of refractory materials, *Interceram,* **2**, 103 – 6, (2012).

[31] Naghizadeh, R., Rezaie, H.R., Golestani-Fard, F.: The influence of composition, cooling rate and atmosphere on the synthesis and thermal stability of aluminum titanate, *Mater. Sci. Eng. B,* **157,** 20 – 5, (2009).

[32] Werner, J., Aneziris, C.G., Dudczig, S.: Young's modulus of elasticity of carbon-bonded alumina materials up to 1450 °C, *J. Am. Ceram. Soc.,* **96**, [9], 2958 – 65, (2013).

[33] Larson, D.R., Coppola, J.A., Hasselman, D.P.H., Bradt, R.C.: Fracture toughness and spalling behavior of high-Al_2O_3 refractories, *J. Am. Ceram. Soc.,* **57**, [10], 417 – 21, (1974).

[34] Risbud, S.H., Pask, J.A.: SiO_2-Al_2O_3 metastable phase equilibrium diagram without mullite, *J. Mater. Sci.,* **13**, 2449 – 54, (1978).

[35] Schulle, W.: Refractory materials, in German. 1st edition. Dt. Verlag für Grundstoffind. Leipzig, 1990.